Real-Time Estimation of Reservoir Influx Rate and Pore Pressure Using a Simplified Transient Two-Phase Flow Model

Adrian Ambrus[1]*, Ulf Jakob Flø Aarsnes[2,5], Ali Karimi Vajargah[3], Babak Akbari[4], Eric van Oort[3] and Ole Morten Aamo[5]

***Corresponding Author**: Adrian Ambrus, Email: aambrus@utexas.edu, phone: +1 (215) 485-2909, address: Department of Mechanical Engineering, The University of Texas at Austin, 204 E. Dean Keeton Street, Stop C2200, Austin TX, 78712.
1: Department of Mechanical Engineering, The University of Texas at Austin.
2: International Research Institute of Stavanger.
3: Department of Petroleum and Geosystems Engineering, The University of Texas at Austin.
4: Craft and Hawkins Department of Petroleum Engineering, Louisiana State University.
5: Department of Engineering Cybernetics, Norwegian University of Science and Technology.

Authors' email:
Ulf Jakob Flø Aarsnes: ujfa@iris.no
Ali Karimi Vajargah: ali.karimi@utexas.edu
Babak Akbari: babak@lsu.edu
Eric van Oort: vanoort@austin.utexas.edu
Ole Morten Aamo: ole.morten.aamo@itk.ntnu.no

Abstract

The ability to perform accurate pore pressure and reservoir inflow estimation during a kick incident is necessary, particularly when drilling in formations with narrow pressure margins. Currently available techniques for pore pressure estimation and reservoir characterization either rely on empirical correlations requiring access to well logging data and other petrophysical information, or require downhole pressure sensing and advanced flow metering capabilities. This paper introduces a model-based estimation technique which uses surface measurements commonly available in a Managed Pressure Drilling (MPD) system, coupled with a simplified transient two-phase model. This model is capable of representing essential dynamics during a gas kick with reduced computational overhead, but without sacrificing significant modeling accuracy. First, the model is validated in a gas kick scenario against experimental data, showing good agreement between key measured parameters and the model predictions, and thereby justifying the model applicability to field operations. Next, data generated from a commercial simulator test case is used to evaluate the proposed estimation methodology. The estimated pore pressure and reservoir productivity are close to their respective values from the commercial simulator, and the flow out rate and surface back-pressure predicted by the simplified two-phase model yield very good match against the simulator results.

1. Introduction

When drilling wells in challenging subsurface environments, such as complex geo-pressured deepwater prospects, it is crucial to maintain the wellbore pressure at a value above both the reservoir pore pressure and the minimum mud pressure required for wellbore stability (or in the case of underbalanced operations, between the wellbore stability limit and the pore pressure). Furthermore, wellbore pressure should not exceed the fracture pressure at any depth in the open-hole section, which effectively limits the available pressure window for safe drilling. Of these pressure limits, the most critical is the pore pressure, as falling below this value in an uncased hole section (e.g. due to insufficient mud weight, poor hydraulics management, improper hole fill-up during tripping or an abnormally pressured zone) leads to influx of formation fluids (oil, water, gas, or a combination thereof) into the wellbore.

Influxes (also known as "kicks") tend to be more hazardous when the formation fluids contain gas, which expands in the annulus causing large variations in annular pressure. An uncontrolled kick triggers a "blow-out", which has potentially catastrophic consequences, impacting rig personnel safety, the surrounding environment, project economics, company and industry reputation (Karimi Vajargah et al., 2014). As a result, the proper planning and execution of well control operations is a major concern in any well being drilled, and the ability to model the gas influx dynamics in real-time, in addition to robustly estimating pore pressure, can significantly improve the success of a well control procedure.

With the development of MPD techniques enabling precise control of the annular pressure profile, wells can be drilled more safely in formations with narrow pressure margins. A particular variant of MPD, which has become more prevalent in recent years, is the constant bottom-hole pressure (CBHP) technique. This method relies on a dedicated choke manifold for applying back-pressure on the annular side, with the goal to maintain the bottom-hole pressure constant throughout the operation. Additionally, CBHP MPD systems include an accurate flow metering system, enabling early kick detection by constant monitoring of return flow in the closed-loop circulation system (Santos et al., 2003). The early kick detection, combined with immediate application of back-pressure by manipulating the size of the choke valve orifice, allows small and medium size kicks to be safely circulated out the of the well without the need for a conventional shut-in operation (Karimi Vajargah et al., 2014; Kinik et al., 2015; Aarsnes et al., 2016a).

In addition to state-of-the art actuation and sensing equipment, the CBHP MPD technique also requires an accurate hydraulic model with multi-phase flow capabilities. Although advanced models have been developed to this end, their complexity makes them impractical for real-time applications such as model-based closed-loop control and estimation. As a result, most MPD control systems in the industry still rely on single-phase dynamic models (e.g. Godhavn, 2010; Kaasa et al., 2012; Reitsma and Couturier, 2012). Therefore, introducing a fit-for-purpose model which can capture the essential dynamics of gas expansion with limited computational expense and complexity is highly desirable. One potential application of such a model is the real-time estimation of pore pressure and reservoir productivity during a kick incident. This paper introduces a model-based estimation methodology employing a simplified two-phase flow model developed by the authors (Ambrus et al., 2015; Aarsnes et al., 2016b). An experimental test data set is first used to validate the model, and subsequently the estimation algorithm is applied on a test case generated using a commercial multi-phase simulator.

2. Background

The proper knowledge of pore pressure, together with fracture pressure and the pressure required for wellbore stability is a primary factor in the design of a well program prior to drilling. Traditional methods for determining pore pressure in a drilling operation rely either on repeat formation tests and drill stem tests, or on empirical correlations to petrophysical logs, such as sonic, density and resistivity logs (Aadnoy et al., 2009). Among the most widely used correlation techniques are Eaton's method, used for estimating pore pressure in shales based on normal compaction trends and resistivity, sonic, or "d-exponent" logs, and Bowers' method, which uses a correlation between sonic velocity and effective stress accounting for the underlying causes of overpressure (Ameen Rostami et al., 2015).

The development of MPD techniques has enabled new approaches to real-time pore pressure estimation during kick incidents. Gravdal et al. (2010) used statistical modeling of the surface back-pressure build-up curve during shut-in to arrive at an estimate of pore pressure. A polynomial curve-fit was used to ascertain the wellbore pressure balanced the formation pressure, such that the measured bottom-hole pressure could be used as the new pore pressure estimate. Application of this algorithm requires a downhole pressure sensor, or an estimate thereof arrived at using a transient model such as the one suggested in this paper. Santos et al. (2003) introduced a method for determining pore and fracture

pressure while drilling through stepwise reduction or increase in surface back-pressure until a micro influx or leak off is detected. Ameen Rostami et al. (2015) showed a more recent application of this technique, where downhole pressure is continuously monitored during the test using a Pressure While Drilling (PWD) tool, and the readings are used to calibrate previous pore pressure estimates, obtained using Eaton's d-exponent method or other similar techniques.

Real-time reservoir characterization has also been facilitated by underbalanced drilling (UBD), where the bottom-hole circulating pressure is intentionally kept below the pore pressure, effectively producing formation fluids while drilling (Vefring et al., 2003). In addition to minimizing reservoir impairment and maximizing production, UBD enables a better understanding of reservoir properties through comparison between real-time production rates and well logging data (Culen and Killip, 2005). Additional information can be inferred from pressure buildup data and gas and liquid flow metering on surface, leading to more accurate estimates of reservoir pressure and productivity index for different reservoir sections (Suryanarayana et al., 2007; Shayegi et al., 2012).

In addition to the methodologies above, which are mostly empirical and/or measurement-intensive, several researchers have attempted model-based estimation techniques, relying on physics-based models of the drilling hydraulics. Zhou et al. (2011) used an adaptive observer in conjunction with a single-phase hydraulic model and a linear reservoir model to estimate influx rate and pore pressure in an MPD system. Their estimation algorithm did not take gas expansion into account, which reduced performance when gas was being circulated out. An adaptive observer was also used by Hauge et al. (2012) for estimating the influx rate as well as the depth of the influx zone. A more sophisticated approach, using an infinite-dimensional boundary observer was applied to a transmission line model of the drilling hydraulics in order to estimate influx or lost circulation events occurring in an MPD setting (Hauge et al., 2013).

In the context of UBD operations, Vefring et al. (2003) used an Ensemble Kalman Filter and the Levenberg-Marquardt method on the Drift-Flux Model coupled with a dynamic reservoir model to estimate reservoir pore pressure and permeability. Biswas et al. (2003) employed a genetic algorithm in conjunction with a transient two-phase reservoir simulator for the problem of estimating reservoir permeability as a function of depth. Aarsnes et al. (2014a) used the Drift-Flux Model in conjunction with an Extended Kalman Filter for on-line estimation of the productivity index, while uncertain model parameters, such as friction factor, choke model coefficients and slip velocity, required off-line calibration.

3. Theory

The methodology presented in this paper comprises a simplified transient two-phase hydraulic simulator (the "reduced Drift Flux Model") and an estimation algorithm which builds upon a reservoir inflow model. The information flow among these key components and their input and output parameters are schematically illustrated in Figure 1. The models and algorithms used are detailed in Section 3.1 and Section 3.2. It should be noted that this approach only requires surface measurements (mud flow rate in and out of the well, pressure at the well head, and pit gain), whereas downhole pressure is computed using the reduced Drift Flux Model.

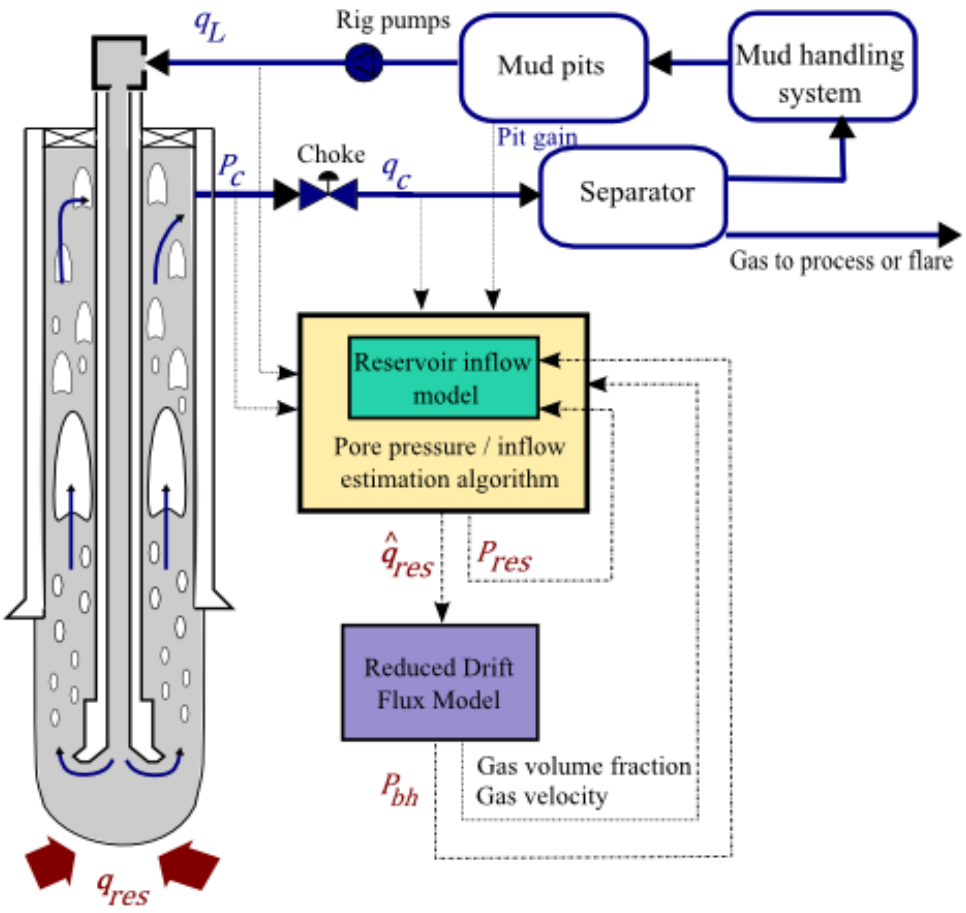

Figure 1. General flow diagram for proposed methodology.

3.1. The Reduced DFM

The Drift-Flux Model (DFM) is one of the multi-phase models most frequently used in drilling applications. The DFM consists of separate mass balance equations and a combined momentum balance, together with several closure relations and a slip relation (see Appendix A for the mathematical formulation). Although widely employed in well control simulation software (e.g. Nickens, 1987; Podio and Yang, 1986; Rommetveit and Vefring, 1991; Petersen et al., 2008), the DFM remains too unwieldy for real-time application in conjunction with model-based estimation and control techniques (Aarsnes, 2016). Finding efficient numerical solutions of the DFM is considered difficult due to strong non-linear coupling mechanisms and challenges associated with transition to single-phase regions (Evje and Wen, 2013). As such, a series of "reduced" DFMs, also called "No Pressure Wave" models, have been suggested (Taitel et al., 1989; Masella et al., 1998; Choi et al., 2013). These models represented attempts to simplify the classical DFM by imposing a quasi-equilibrium momentum balance, with the goal of simplifying the resulting model equations. The use of these models has been justified for applications where the relatively slow gas propagation dynamics are more important than the fast pressure dynamics (Aarsnes et al., 2015). For applications such as MPD, where the transient evolution of the wellhead pressure as controlled by the back-pressure choke is of importance, a relation giving the dynamics of the pressure at the boundary is required. The proposed reduced DFM addresses this issue by adding a first-

order ordinary differential equation representing the pressure dynamics (Eq. 2), coupled with a transport equation for the propagation of the void fraction (α_G) through the well (Eq. 1).

In this paper we employ the model presented in Aarsnes et al. (2016b), augmented with the slip law of Shi et al. (2005) to improve performance when compared to full-scale wellbore operations. The model formulation is summarized below, with a detailed derivation outlined in Appendix A:

$$\frac{\partial \alpha_G}{\partial t} + v_G \frac{\partial \alpha_G}{\partial x} = E_G + \Gamma_G^* - \Gamma_L^* , \tag{1}$$

$$\frac{dP_c}{dt} = \frac{\bar{\beta}}{V}(q_L + q_G - q_c + T_{XE}), \tag{2}$$

where:

$$E_G = -\frac{\alpha_G(1 - C_0\alpha_G)}{\gamma P}\left(\frac{dP_c}{dt} + v_G\bar{S}\right), \tag{3}$$

$$\Gamma_G^* \equiv \frac{(1 - C_0\alpha_G)\,\Gamma_G}{\rho_G}, \qquad \Gamma_L^* \equiv \frac{\mathrm{C_0\alpha_G\Gamma_L}}{\rho_L}, \tag{4}$$

$$\bar{\beta} \equiv \frac{\beta_L}{1 + \frac{\beta_L}{V}\int_0^L \frac{C_0\alpha_G}{\gamma P} A dx}, \tag{5}$$

$$T_{XE} \equiv A(v_G(L) - v_{G0}), \tag{6}$$

$$v_{G0} = C_0\frac{q_G + q_L}{A} + v_\infty. \tag{7}$$

The model formulation is completed by the following closure relations:

$$P(x) = P_c + \int_L^x \bar{S}(\xi)d\xi, \tag{8}$$

$$\frac{\partial P}{\partial x} = \bar{S}(x) = -(\rho_L a_L + \bar{\rho}_G\alpha_G)\left[g cos\theta(x) + \frac{2f(q_G + q_L)|q_G + q_L|}{A^2 D}\right], \tag{9}$$

$$v_G(x) = e^{-I_v(x)}\left(v_{G0} + C_0\int_0^x \left[\frac{c_G^2(\zeta)}{\gamma P(\zeta)}\Gamma_G(\zeta) + \frac{\Gamma_L(\zeta)}{\rho_L}\right] e^{I_v(\zeta)}d\zeta\right), \tag{10}$$

$$I_v(x) = \int_0^x \frac{C_0\alpha_G(\xi)}{\gamma P(\xi)}\bar{S}(\xi)d\xi, \tag{11}$$

and, finally, the boundary condition

$$\alpha_G(0,t) = \frac{q_G}{A v_{G0}}. \tag{12}$$

The present formulation assumes that the influx is pure gas, and should thus be used only for drilling operations where gas kicks are expected. Also, mass transfer is not considered, limiting the model use to water-based drilling fluids, where the effects of gas dissolution are generally negligible (Karimi Vajargah, 2013). Additionally, due to the simplifying assumptions in the derivation of the gas dynamics, the formulation does not handle scenarios where the well is completely shut-in (i.e. with both the blow-out preventers and choke closed), as it can prescribe only one boundary condition (Eq. 12). In a shut-in case, an additional boundary condition is required to accommodate a zero net flow rate at the well head. This limitation can however be avoided if the slip velocity is low enough (or the well long enough) such that the gas bubble does not reach the well head before the circulation is resumed and the well control choke is opened. Furthermore, this is not an issue for dynamic well control operations in CBHP MPD, where up to a certain kick size, a complete shut-in is not required to safely bring the well back to overbalance.

For use in back-pressure MPD scenarios, the model can be augmented with an equation relating the choke flow rate to the back-pressure and gas amount going through the choke (Aarsnes et al., 2014b):

$$q_c = \frac{C_v z}{\sqrt{\rho_L}} \sqrt{P_c - P_s} + \left[\left(1 - \sqrt{\frac{\rho_G}{\rho_L}} \frac{1}{Y} \right) A v_G \alpha_G \right] \Bigg|_{x=L}. \tag{13}$$

3.2. Pore Pressure and Reservoir Inflow Estimation

In this section, we present an approach for estimating the inflow rate and pore pressure of the flowing zone based on drilling parameters recorded during a kick. This requires a fit-for-purpose hydraulics model and a reservoir model, which correlates flow from the reservoir to the pressure drawdown, and also to a productivity index, a lumped parameter which is affected by the length of exposed zone, reservoir permeability, porosity, skin factor, reservoir fluid viscosity and compressibility (Vefring et al., 2003). For this application, we are more interested in the qualitative relationship between inflow rate, productivity and pore pressure, thus we use a qualitatively correct, linear inflow relationship (Shayegi et al., 2012):

$$q_{res} = J(P_{res} - P_{bh}), \tag{14}$$

with P_{res} the reservoir pressure, P_{bh} the bottom-hole pressure, and J the productivity index (PI). In the above, it is assumed that $P_{res} > P_{bh}$ (i.e. the well is underbalanced), otherwise, q_{res} is set to zero. Eq. 14 can be recast in a form more amenable for parameter estimation:

$$q_{res} = \phi^T X, \tag{15}$$

where $X = \begin{bmatrix} JP_{res} \\ J \end{bmatrix}$ is the vector of unknown or uncertain parameters and $\phi = \begin{bmatrix} 1 \\ -P_{bh} \end{bmatrix}$ is the regressor. Since, for a kick incident, q_{res} is not directly measured, we will instead use an estimate, $\hat{q}_{res}$.

As a baseline, we can compute $\hat{q}_{res}$ from the instantaneous mud flow out rate minus the mud injection rate, however, this is susceptible to measurement noise (particularly flow out), and does not account for dynamics due to pressure changes and gas expansion as the kick is circulated. Therefore, we employ the

first-order pressure dynamics from Eq.2, where we use $\hat{q}_{res}$ in place of the gas source term q_G and we isolate all terms which explicitly depend on $\hat{q}_{res}$ (Note: in the following, all parameters which are estimated or derived from estimated quantities are denoted with a "^" above their symbol)

$$\frac{dP_c}{dt} = \frac{\hat{\beta}}{V}[q_L - q_c + \hat{q}_{res} + I_0 + 2(q_L + \hat{q}_{res})^2 I_1], \tag{16}$$

with

$$I_0 = \int_0^L \frac{C_0 \hat{\alpha}_G}{\gamma \hat{P}} \hat{v}_G \hat{\rho}_m \, g cos(\theta) A dx, \tag{17}$$

$$I_1 = \int_0^L \frac{C_0 \hat{\alpha}_G}{\gamma \hat{P}} \hat{v}_G \hat{\rho}_m \, \frac{f}{AD} \, dx, \tag{18}$$

where I_0, I_1 account for gas expansion due to the hydrostatic and frictional pressure gradients, respectively. Note in the above that $\hat{v}_G$ is computed from Eq. 10 with $\Gamma_L = \Gamma_G = 0$ and the quantities $\hat{\beta}, \hat{P}(x), \hat{v}_G(x), \hat{\alpha}_G(x)$ are also estimates of the true values as they all depend on $\hat{q}_{res}$. For MPD scenarios, where kick size is usually limited, we can assume $q_{res}^2 \ll q_L^2$, and thus neglect the quadratic $\hat{q}_{res}$ term in Eq. 16, which yields:

$$\frac{dP_c}{dt} = \frac{\hat{\beta}}{V}[q_L - q_c + I_0 + 2q_L^2 I_1 + \hat{q}_{res}(1 + 4q_L I_1)]. \tag{19}$$

Eq. 19 above can be low-pass filtered to remove noise in the measurements, and also to allow a mathematical formulation which enables linear regression techniques. Using Laplace transform notation for the low-pass filter transfer function, $F(s) = \frac{1}{\tau s + 1}$, we have:

$$\frac{s}{\tau s + 1} P_c - \frac{1}{\tau s + 1} \frac{\hat{\beta}}{V}[q_L - q_c + I_0 + 2q_L^2 I_1] = \frac{1}{\tau s + 1} \left\{ \frac{\hat{\beta}(1 + 4q_L I_1)}{V} \, \phi^T X \right\}. \tag{20}$$

Denoting the left-hand side of Eq. 20 by y and the term $\frac{1}{\tau s + 1} \left\{ \frac{\hat{\beta}(1 + 4q_L I_1)}{V} \, \phi \right\}$ by ψ allows us to finally write a linear equation of the form $y = \psi^T X$, which can be solved using an on-line regression technique, such as recursive least squares (RLS) (Ljung 1999). Details of the RLS implementation are provided in Appendix C. Using the notation above, an alternate approach to estimating influx rate is by computing the instantaneous estimate:

$$\hat{q}_{res}^{inst} = \frac{Vy}{\hat{\beta}(1 + 4q_L I_1)}. \tag{21}$$

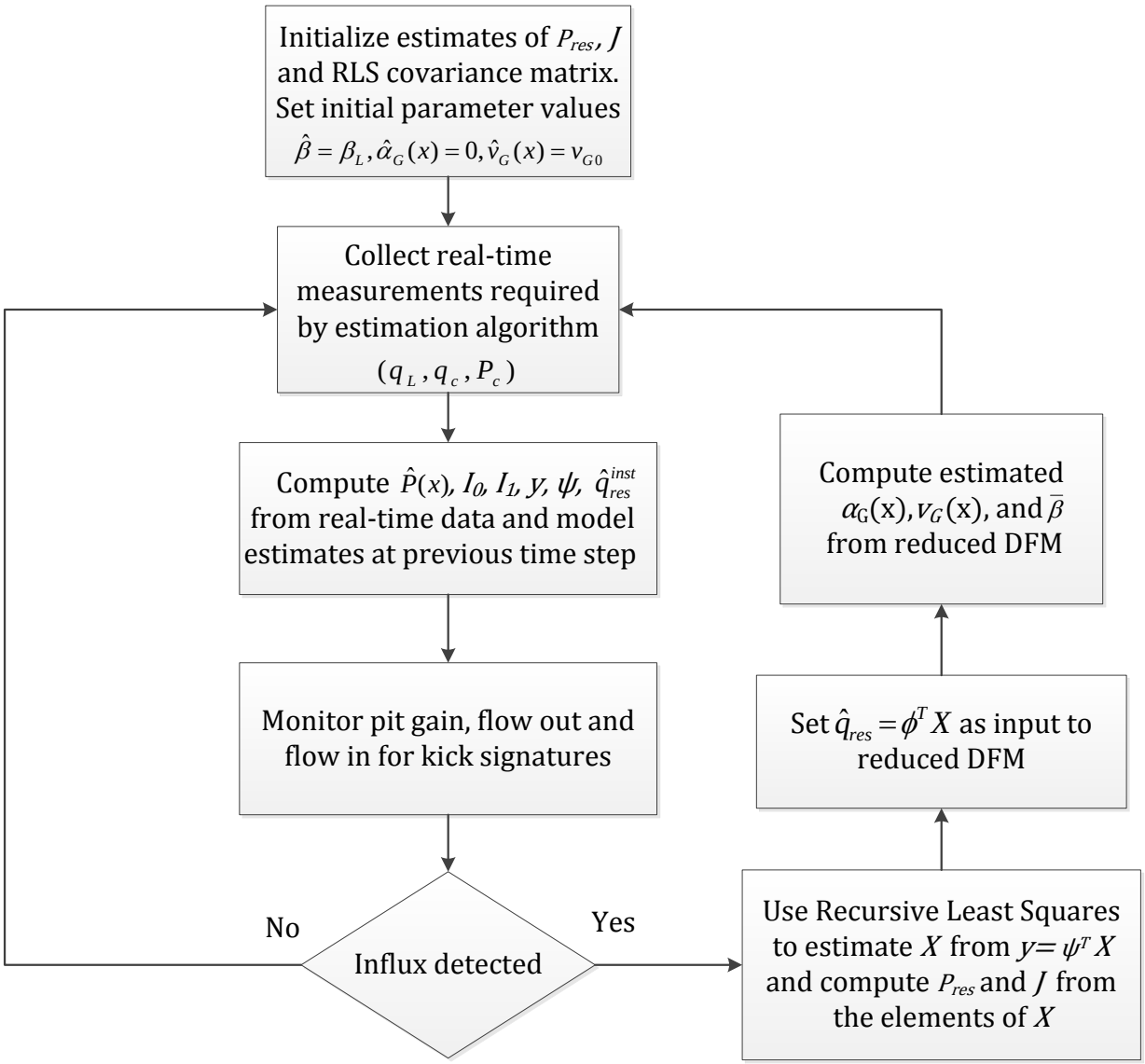

Figure 2. Detailed flowchart for pore pressure and reservoir inflow estimation methodology.

The estimation methodology is summarized in Figure 2. While advanced kick detection techniques are beyond the scope of this work, a simple, threshold-based methodology was applied on the measured pit gain and differential flow rate (i.e. return flow minus flow in rate). Since the reservoir model (Eq. 14) is only valid while the well is underbalanced, the RLS algorithm can only be applied over the time window starting from the detection of the kick up to the point when the well reaches an overbalanced state. Thus, in order to ensure the estimated parameters do not diverge, the RLS module needs to be stopped as soon as influx from the formation ceases, which the proposed algorithm infers when the differential flow rate and the pit gain both decrease below specified thresholds (values for these thresholds and other design parameters used in the simulations in Section 4 are given in Table 1). As the gas percolates in the annular space, a slow increase in flow out rate and pit gain are still observed, but their rate of change is much slower than when the kick enters the wellbore, and should not be misinterpreted as additional influx.

Table 1. Design parameters for RLS estimation algorithm.

Parameter	Value	Parameter	Value
Pit gain kick detection threshold	0.5 barrels	Initial estimate of reservoir pressure ($\hat{P}_{res}(0)$)	Hydrostatic pressure + 150 psi
Differential flow rate kick detection threshold	10 gal/min	Initial estimate of reservoir PI	1.46 ft^3/min/psi
Pit gain kick stop threshold	0.1 barrels	Initial value of RLS regressor ($\psi(0)$)	$\frac{\beta_L}{V}\begin{bmatrix}1\\-\hat{P}_{res}(0)\end{bmatrix}$
Differential flow rate kick stop threshold	1 gal/min	Initial value of RLS covariance matrix	$2(\psi(0)^T\psi(0)+\boldsymbol{I})^{-1}$
Low-pass filter time constant ($\boldsymbol{\tau}$)	10 seconds	RLS forgetting factor	1

4. Results and Discussion

4.1. Validation of Reduced DFM

The model described in Section 3.1 was validated on an experimental data set obtained from a well control test conducted at Louisiana State University. The test setup, illustrated in Figure 3, was detailed by Chirinos et al. (2011). An 11-bbl gas kick was simulated by injecting natural gas inside the 1.25-in tubing while water-based mud was continuously pumped through the annulus formed by the 3.5-in drill pipe and the 1.25-in tubing, with returns taken through the annulus between the 9.625-in casing and the 3.5-in drill pipe. A manually operated choke manifold was used to provide back-pressure, with the goal of keeping a constant standpipe pressure throughout the gas circulation. The mud circulation and gas injection rate recorded during the test were used as inputs to the model and are shown in Figure 4. Well geometry, mud properties and other model inputs are detailed in Table 2. Since there was no down-hole pressure measurement in the experimental setup, the bottom-hole pressure was inferred from the standpipe pressure and flow in rate according to the following formula (Guo and Liu, 2011):

$$P_{bh} = P_d + \rho_L g h - \frac{2 f_d \rho_L q_L^2}{{A_d}^2 D_d} L \tag{22}$$

where P_d is the recorded standpipe pressure and f_d is the drill pipe friction factor, calculated using the correlations for yield-power law fluids detailed in Ahmed and Miska (2009).

The reduced DFM was implemented using an explicit, first-order finite difference scheme (see Appendix D for the numerical implementation details) with a time step of 1 second and 200 grid cells. The simulation results were compared to flow out and pit gain data (Figure 5) as well as casing pressure data recorded from the experiment (Figure 6), showing excellent match for pressure and reasonable agreement for the pit gain and flow out, as indicated by the figures and also the average percent errors in Table 3. For flow out, the average percent error was computed until the point when gas reached the surface at 100 minutes. After that point, the measured flow out rate was zero, while the recorded pit gain, shown in the lower plot in Figure 5, started decreasing about five minutes later, and the slow pit volume decrease (which was similar in both the measurement and model prediction) suggested that flow out rate could not have been zero. Based on this observation, it can be inferred that the reduced DFM predicts the correct

flow out rate, whereas the flow meter may have not been properly calibrated for two-phase flow. Consequently, the flow out data can be used for validating the model only when all the flow through the meter is in a liquid phase, which is the case until gas reaches the surface.

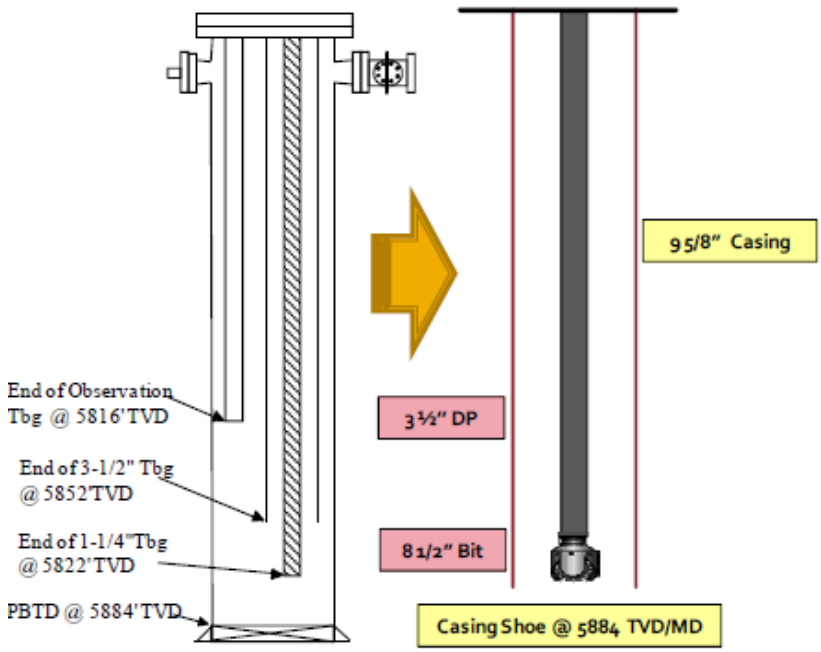

Figure 3. Louisiana State University well schematic (from Chirinos et al., 2011).

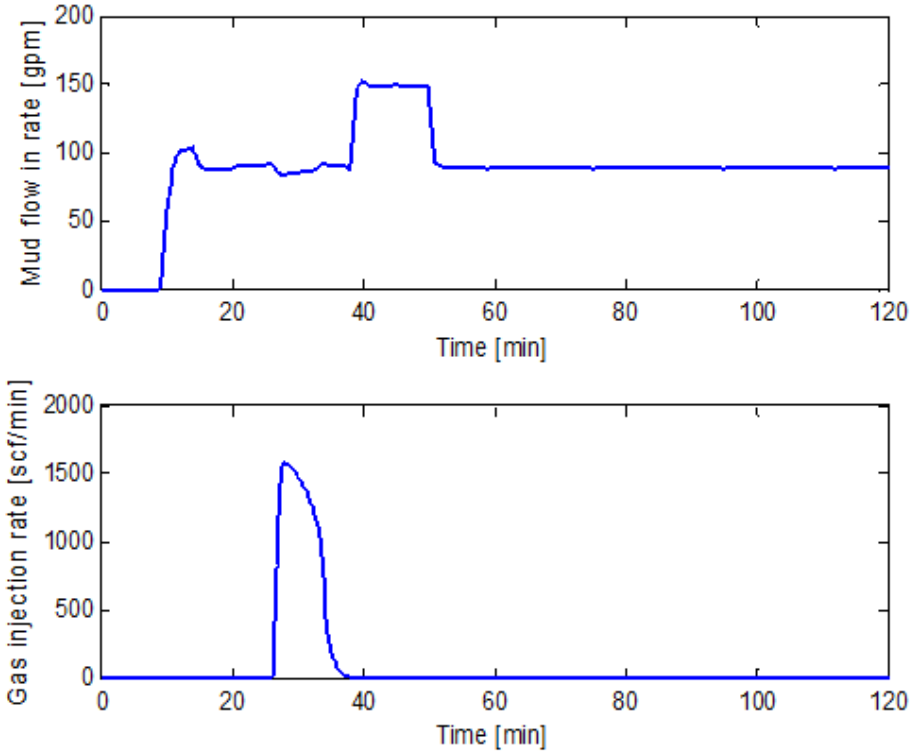

Figure 4. Mud flow in rate (upper) and gas injection rate (lower) from well control test.

Table 2. Input parameters for simulation on experimental data set.

Parameter	Value	Parameter	Value
Well measured depth	5,884 ft	Mud weight	8.6 lbm/gal
True vertical depth	5,884 ft	Plastic viscosity	8 cP
Casing shoe depth	5,884 ft	Yield point	2 lbf/(100ft^2)
Casing size	9.625 in	Bulk modulus	2.15x10^5 psi
Drill pipe outer diameter	3.5 in	Choke valve coefficient	0.107 ft^2
Drill pipe inner diameter	2.6 in	Choke gas expansion factor	0.25
Gas injection tubing diameter	1.25 in	Surface temperature	93 °F
Mud circulation rate	90-150 gal/min	Bottom-hole temperature	140 °F

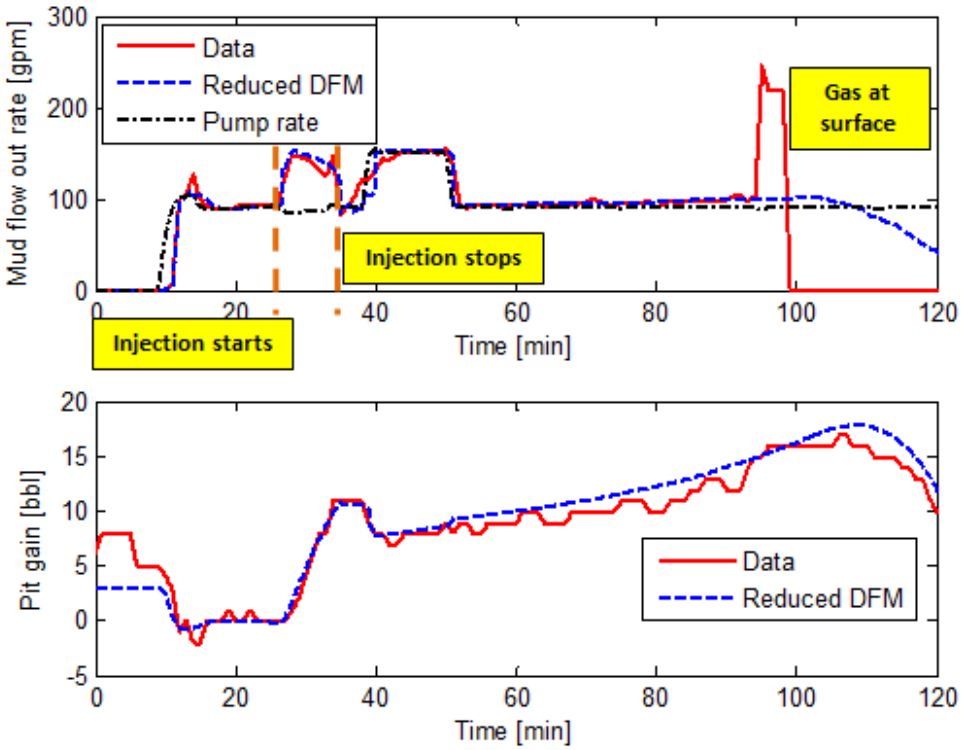

Figure 5. Comparison of experimental data with the reduced DFM, mud flow out (upper) and pit gain (lower).

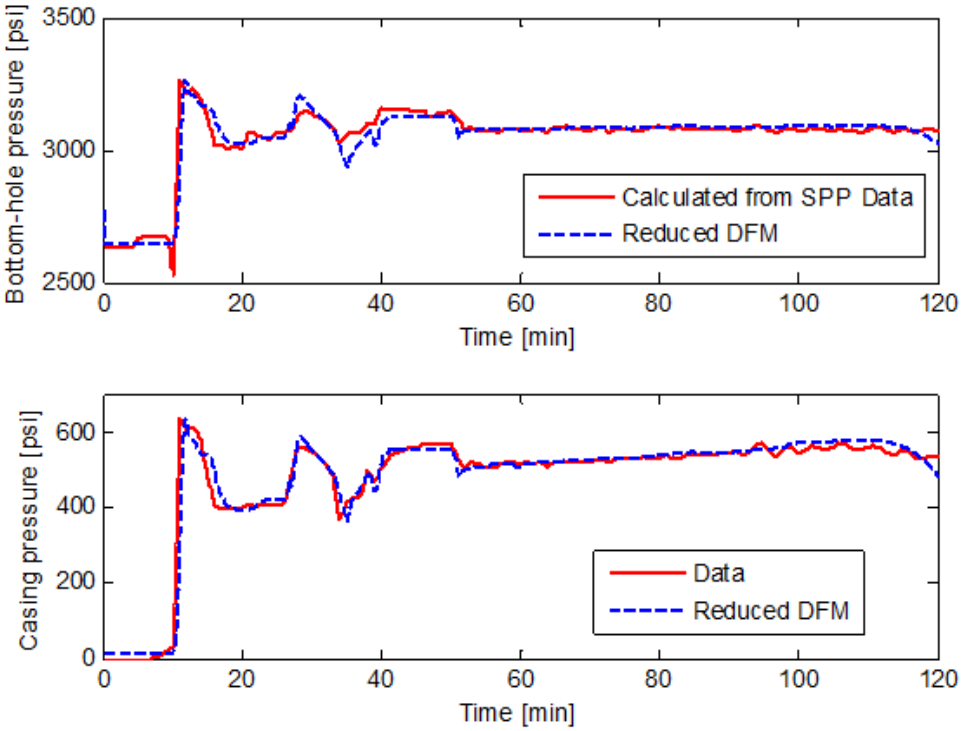

Figure 6. Comparison of experimental data with the reduced DFM, bottom-hole pressure (upper) and casing pressure (lower).

Table 3. Average percent error between experimental data and reduced DFM.

Parameter	Average percent error (%)
Bottom-hole pressure	0.5
Casing pressure	1.9
Flow out rate	8.6
Pit gain	10.4

4.2. Pore Pressure and Reservoir Inflow Estimation Results

The pore pressure and reservoir inflow estimation methodology from Section 3.2 was tested on an MPD well control scenario generated using the commercial multi-phase simulator OLGA (Bendiksen et al., 1991). The simulated case consisted of a 12,100-ft vertical land well with 9.625-in casing set up to 8,000 ft and 3-in drill pipe extending down to the total depth. The simulation inputs are detailed in Table 4. A 12-lbm/gal Newtonian water-based mud was circulated at a constant rate of 200 gal/min. At 12,090 ft the well intersected a dry gas reservoir with an average pore pressure of 7,750 psi, and a linear PI model was used to simulate the reservoir influx. The initial underbalance of 300 psi resulted in a 10-bbl kick taken over a period of 10 minutes. The choke opening was then adjusted using the built-in controller in OLGA to maintain a target bottom-hole pressure of 7,900 psi.

Table 4. Input parameters for OLGA simulation.

Parameter	Value	Parameter	Value
Well measured depth	12,100 ft	Plastic viscosity	30 cP
True vertical depth	12,100 ft	Yield point	0
Casing shoe depth	8,000 ft	Bulk modulus	$3x10^5$ psi
Casing size	9.625 in	Reservoir pore pressure	7750 psi
Hole / bit size	8.5 in	Reservoir productivity index	0.022 ft^3/min/psi
Drill pipe outer diameter	3 in	Choke valve coefficient	0.0694ft^2
Drill pipe inner diameter	2.5 in	Choke gas expansion factor	0.3
Mud circulation rate	200 gal/min	Surface temperature	60 °F
Mud weight	12 lbm/gal	Bottom-hole temperature	150 °F

During the RLS estimation, measured flow out and back-pressure were fed back to the algorithm for determining q_{res}, but after the influx ceased, the model was run in feedforward mode with q_{res} set to zero, thus allowing comparison of predicted flow out and back-pressure to their measurements. The flow rate out trend is shown in the upper plot of Figure 7, indicating very good match with the OLGA data. The lower plot in Figure 7 gives the estimate of the gas influx rate, with both the RLS and instantaneous result. It should be noted that both show good agreement with the OLGA values during the kick, but once the influx stops, the instantaneous estimate starts to drift away from zero. This is a consequence of the difference between the predicted mud flow out rate and the OLGA data. That is, after the kick is known to have stopped, the instantaneous estimate can be used to gauge the correctness of the model prediction. The RLS estimate, on the other hand, is formulated directly from the reservoir model and will be equal to zero when the bottom-hole pressure exceeds the estimated pore pressure, and greater than zero, otherwise. This information will be useful to predict the size of secondary influxes which may arise, for instance, due the MPD system applying insufficient back-pressure while the kick is being circulated.

Figure 8 shows the estimates of pore pressure and PI, which converge in the proximity of the actual values (pore pressure estimate converged within 30 psi of the OLGA input, which is reasonable accuracy for practical purposes). This error can be further reduced if P_{bh} is directly measured from PWD equipment, if such equipment is available and data sampling rates are sufficiently high, instead of being computed from the reduced DFM. It should be noted that the RLS algorithm was started after an initial pit gain of 0.5 bbl, which is sufficiently early to capture the magnitude of the influx, however, if higher thresholds are used for starting the algorithm, some of the gas entering the well would not be accounted for by the model, leading also to larger estimation errors. The low pit gain threshold for starting the RLS should not be an issue for MPD systems, where high-accuracy flow instrumentation enables kick detection at very low influx volumes ("micro influxes") (Santos et al., 2003). Alternately, the RLS may be turned on before a kick is confirmed, and if the estimates are seen to diverge, the algorithm can be re-started. Also, the instantaneous influx rate estimate (Eq. 21), which is continuously updated, may be used as input to the reduced DFM before the influx is confirmed by the detection algorithm. Finally, Figure 9

shows the comparison of OLGA pressure data to the values predicted by the reduced DFM, displaying good agreement as well.

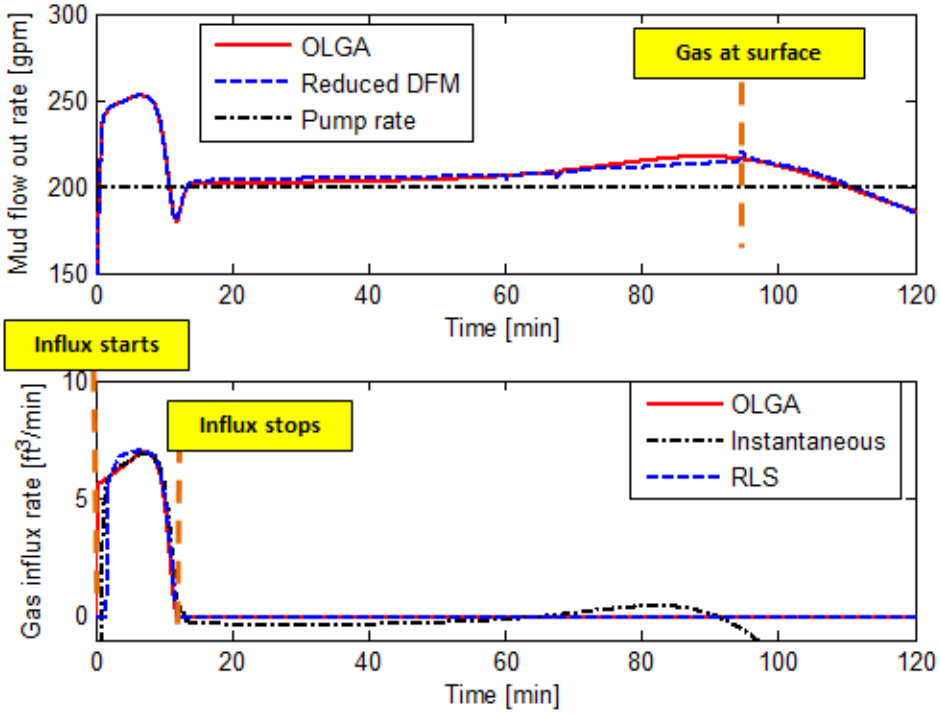

Figure 7. Mud flow rate out from OLGA and predicted by the reduced DFM (upper); estimated gas influx rate (lower).

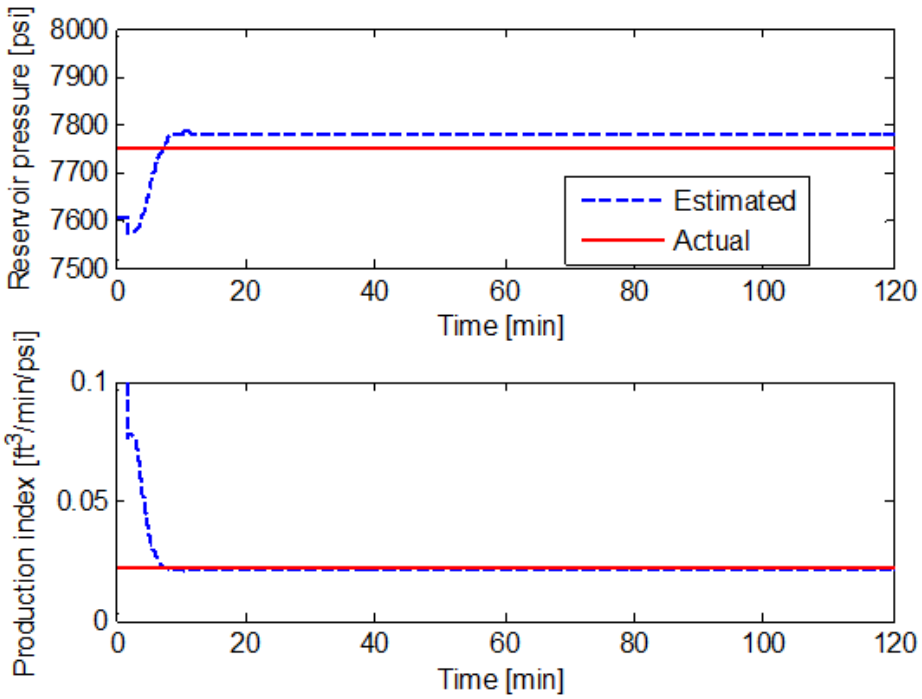

Figure 8. Reservoir pore pressure (upper) and PI (lower) estimated by the RLS algorithm. Actual values are the OLGA simulation inputs.

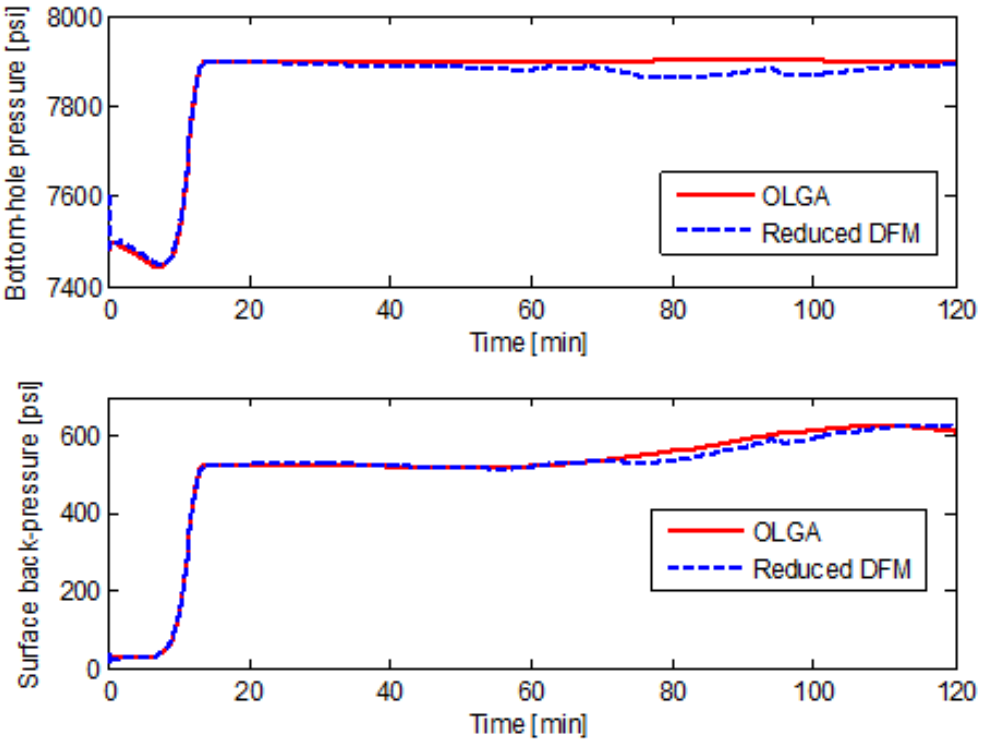

Figure 9. Bottom-hole pressure from OLGA and predicted by the reduced DFM (upper); surface back-pressure from OLGA and predicted by reduced DFM (lower).

One of the main advantages of this approach, compared to currently available methods for real-time pore pressure determination while drilling, is that it does not require intentional reduction of back-pressure to ascertain the pore pressure value. The algorithm can be running in the background during normal MPD operations and does not interfere with existing well control procedures and kick detection systems. While this paper is focused on gas kick scenarios, the methodology presented can be extended to oil or water kicks, with the appropriate modifications to the reduced DFM, particularly to the slip law and equation of state (see Eqs. A6 and A8 in Appendix A). To this end, logic for determining the influx type (e.g. Karimi Vajargah et al., 2014) and robust kick detection algorithms (e. g. Pournazari et al., 2015) may be added to the current approach. It is further noted that a linear reservoir inflow model was employed in the present formulation; however, it should be possible to extend the algorithms to accommodate more general, non-linear inflow models (Wiggins et al., 1996), which require the application of non-linear regression techniques.

5. Summary and Conclusions

- This paper presents a novel approach for estimating pore pressure and reservoir inflow rates during gas kick events in Managed Pressure Drilling operations. The algorithm leverages a simplified transient two-phase wellbore flow model coupled with a reservoir inflow model, and a Recursive Least Squares regression technique.
- The two-phase flow model consists of a transport equation governing the gas dynamics, coupled with an ordinary differential equation representing pressure dynamics in response to changes in choke opening. These equations yield a reduced Drift-Flux Model that can capture the essential two-phase dynamics during a gas kick with less numerical complexity compared to high-fidelity

simulators. This allows for a fast, explicit numerical solution scheme, which is suitable for real-time implementation in automatic control and estimation applications.

- The model was successfully validated on experimental data from a test well where a kick was simulated through controlled gas injection. Very good agreement was observed between the measured and the modeled casing pressure and pit gain, and also between the bottom-hole pressure predicted by the model and the value derived from the standpipe pressure measurements.
- A low-pass filtered version of the pressure dynamics equation from the reduced DFM is used for dynamic estimation of the reservoir inflow rate, pore pressure and reservoir productivity from real-time pressure and flow data. The algorithm only requires surface sensor measurements and does not interfere with well control procedures. It presents an advantage over existing methods for dynamic pore pressure testing in MPD, as it does not require surface back-pressure to be intentionally reduced until influx is observed.
- The estimation methodology was tested on a MPD gas kick scenario generated with a commercial multi-phase simulator. The algorithm was able to estimate pore pressure within 30 psi of the actual value, and also the estimated influx rate and reservoir productivity index were matched closely. The estimated kick size was then input to the reduced DFM to predict the flow rate out and back-pressure during the kick circulation, which gave a very good match with actual values from the simulator.
- In the proposed algorithm, it is possible to compute the influx rate either directly from the RLS estimates of reservoir pressure and productivity index, or as an instantaneous value based on low-pass filtered surface measurements. In the simulation scenario, both approaches gave accurate influx rate predictions while flow from the formation was active, but the instantaneous value was shown to drift away from zero once the influx stopped. While the instantaneous value is useful for evaluating the validity of the model prediction, for practical application, it is recommended not to use the instantaneous value once the well is overbalanced so as to avoid mistakenly inferring that additional kicks are taken.

Acknowledgements

The authors gratefully acknowledge Wesley Williams from the Petroleum Engineering Research and Technology Transfer Laboratory at Louisiana State University, Koray Kinik from Weatherford International, and the Drilling and Rig Automation Group at The University of Texas at Austin for their valuable comments. Schlumberger is also thanked for providing the OLGA license. The work of the first, third and fifth authors was supported by the RAPID (Rig Automation and Performance Improvement in Drilling) sponsor group (ExxonMobil, Sinopec, Baker Hughes and NOV). The work of the second and last authors was supported by Statoil ASA and the Research Council of Norway (NFR project 210432/E30 Intelligent Drilling). Parts of the work of the second author was sponsored by the Research Council of Norway, ConocoPhillips, Det Norske Oljeselskap, Lundin, Statoil and Wintershall through the research center DrillWell (Drilling and Well Centre for Improved Recovery) at IRIS.

Nomenclature

Abbreviations

CBHP = Constant Bottom-Hole Pressure
DFM = Drift-Flux Model
MPD = Managed Pressure Drilling
PI = Productivity Index

PWD = Pressure While Drilling
RLS = Recursive Least Squares
SBP = Surface Back-Pressure
SPP = Standpipe Pressure
UBD = Underbalanced Drilling

Symbols

A = Wellbore cross-sectional area (m^2)
A_d = Drill pipe cross-sectional area (m^2)
c_G = Velocity of sound in gas (m/s)
C_v = Choke valve coefficient (m^2)
C_0 = Slip law profile parameter
D' = Dimensionless wellbore hydraulic diameter
D = Wellbore hydraulic diameter (m)
D_d = Drill pipe hydraulic diameter (m)
E_G = Local gas expansion rate (1/s)
f = Wellbore friction factor
f_d = Drill pipe friction factor
F = Low-pass filter
g = Gravitational constant (m/s^2)
h = Well true vertical depth (m)
i = Cell index in numerical scheme
$\boldsymbol{I}$ = Identity matrix
I_0 = Gas expansion variable due to hydrostatic term (m^3/s)
I_1 = Gas expansion variable due to frictional term (s/m^3)
I_v = Integral in gas velocity gradient equation
J = Reservoir productivity index ($m^3/s/Pa$)
L = Well measured depth (m)
n = Time index in numerical scheme
N = Number of grid cells in numerical scheme
P = Pressure (Pa)
$\boldsymbol{P}$ = RLS covariance matrix
q = Volumetric flow rate (m^3/s)
R_G = Ideal gas constant (J/kg/K)
s = Laplace variable
S = Source term in momentum balance equation (Pa/m)
$\bar{S}$ = Approximated source term in momentum balance (Pa/m)
t = Time (s)
Δt = Time step in numerical scheme (s)
T = Wellbore temperature (K)
T_{E_G} = Total volumetric gas expansion rate (m^3/s)
T_{XE} = Pressure dynamics source term due to gas expansion (m^3/s)
v = Fluid velocity (m/s)
v_{cr} = Characteristic velocity in slip model (m/s)
v_∞ = Slip velocity (m/s)
V = Wellbore volume (m^3)

x = Position along wellbore (m)
Δx = Cell size in numerical scheme (m)
X = Vector of estimated parameters in RLS algorithm
y = Output of RLS equation
Y = Choke gas expansion factor
z = Choke opening
Z_G = Gas compressibility factor

Greek letters

α = Volume fraction
α_L^* = Slip law profile parameter
β_L = Liquid bulk modulus (Pa)
$\bar{\beta}$ = Effective bulk modulus of gas-liquid mixture (Pa)
γ = Gas adiabatic constant
Γ = Source term in mass balance equation (kg/m^3/s)
Γ^* = Normalized mass balance source term (1/s)
ϕ = Regressor in RLS estimation
ψ = Filtered regressor in RLS estimation
ϵ = Convenience variable in RLS algorithm
λ = RLS forgetting factor
ρ = Density (kg/m^3)
$\bar{\rho}$ = Approximated density (kg/m^3)
σ = Gas-liquid interfacial tension (N/m)
θ = Well inclination (rad)
τ = Low-pass filter time constant (s)
ξ, ζ = Dummy variables in integrals and summations

Subscripts

bh = bottom-hole
c = choke/casing
d = drill pipe
G = gas
L = liquid
m = mixture
res = reservoir
s = separator

Superscripts

inst = instantaneous

Accents

$\hat{x}$ = Estimated variable
$\bar{x}$ = Approximated variable

SI Metric Conversion Factors

bbl × 1.589 873	E-01 = m^3
cP × 1.0	E-03 = Pa·s
ft × 3.048	E-01 = m
(°F - 32)/1.8	E+00 = °C
gal × 3.785 412	E-03 = m^3
in. × 2.54	E-02 = m
lbf × 4.448 222	E+00 = N
lbm × 4.535 924	E-01 = kg
psi × 6.894 757	E+03 = Pa

References

Aadnoy, B.S., Cooper, I., Miska, S.Z., Mitchell, R.F., and Payne, M.L (2009). Advanced Drilling and Well Technology. Society of Petroleum Engineers.

Aarsnes, U. J. F. (2016). Modeling of Two-Phase Flow for Estimation and Control of Drilling Operations. PhD Thesis. Norwegian University of Science and Technology.

Aarsnes, U. J. F., Acikmese, B., Ambrus, A., and Aamo, O. M. (2016a). Robust Controller Design for Automated Kick Handling in Managed Pressure Drilling. Journal of Process Control. Submitted.

Aarsnes, U. J. F., Ambrus A., Karimi Vajargah, A., Aamo, O. M. and van Oort, E. (2016b). A Simplified Two-Phase Flow Model Using a Quasi-Equilibrium Momentum Balance. International Journal of Multiphase Flow. Submitted.

Aarsnes, U. J. F., Ambrus A., Karimi Vajargah, A., Aamo, O. M. and van Oort, E. (2015, October). A Simplified Gas-Liquid Flow Model for Kick Mitigation and Control During Drilling Operations. Proceedings of the ASME 2015 Dynamic Systems and Control Conference.

Aarsnes, U. J. F., Di Meglio, F., Aamo, O. M., and Kaasa, G.-O. (2014a, April). Fit-for-Purpose Modeling for Automation of Underbalanced Drilling Operations. SPE/IADC Managed Pressure Drilling and Underbalanced Operations Conference and Exhibition. Madrid, Spain: Society of Petroleum Engineers. doi:10.2118/168955-MS.

Aarsnes, U. J. F., Di Meglio, F., Evje, S., and Aamo, O. M. (2014b, October). Control-Oriented Drift-Flux Modeling of Single and Two-Phase Flow for Drilling. Proceedings of the ASME 2014 Dynamic Systems and Control Conference, Volume 3.

Ahmed, R., Miska, S.Z. (2009). Advanced Wellbore Hydraulics. In: Aadnoy, B.S. (Ed.), Advanced Drilling and Well Technology. Society of Petroleum Engineers, pp. 191-219 (chapter 4.1).

Ahmed, T. (2006). Reservoir Engineering Handbook, Third Edition. Gulf Professional Publishing.

Ambrus, A., Aarsnes, U. J. F., Karimi Vajargah, A., Akbari, B. and van Oort, E. (2015, December). A Simplified Transient Multi-Phase Model for Automated Well Control Applications. International Petroleum Technology Conference, Doha, Qatar. doi:10.2523/IPTC-18481-MS.

Ameen Rostami, S., Kinik, K., Gumus, F., & Kirchhoff, M. (2015, May 4). Dynamic Calibration of the Empirical Pore Pressure Estimation Methods Using MPD Data. Offshore Technology Conference. doi:10.4043/25953-MS.

Bendiksen, K. H., Maines, D., Moe, R., and Nuland, S. (1991, May 1). The Dynamic Two-Fluid Model OLGA: Theory and Application. Society of Petroleum Engineers Production Engineering. doi:10.2118/19451-PA.

Bhagwat, S.M., Ghajar A.J. (2014, February). A flow pattern independent drift flux model based void fraction correlation for a wide range of gas–liquid two phase flow, International Journal of Multiphase Flow, Volume 59, Pages 186-205, ISSN 0301-9322,

Biswas, D., Suryanarayana, P. V., Frink, P. J., & Rahman, S. (2003, October 5-8). An Improved Model to Predict Reservoir Characteristics During Underbalanced Drilling. SPE Annual Technical Conference and Exhibition, Denver, Colorado. Society of Petroleum Engineers. doi:10.2118/84176-MS.

Chirinos, J. E., Smith, J. R., and Bourgoyne, D. A. (2011, January 1). A Simplified Method to Estimate Peak Casing Pressure During MPD Well Control. SPE Annual Technical Conference and Exhibition, Denver, Colorado. Society of Petroleum Engineers. doi:10.2118/147496-MS.

Choi, J., Pereyra, E., Sarica, C., Park, C., Kang, J.M. (2012). An Efficient Drift-Flux Closure Relationship to Estimate Liquid Holdups of Gas-Liquid Two-Phase Flow in Pipes. Energies, *5*, 5294-5306.

Choi, J., Pereyra, E., Sarica, C., Lee, H., Jang, I. S., and Kang, J. (2013, February). Development of a fast transient simulator for gas–liquid two-phase flow in pipes. Journal of Petroleum Science and Engineering. 102, pp. 27–35.

Culen, M. S., & Killip, D. R. (2005, May 25-27). Forensic Reservoir Characterisation Enabled with Underbalanced Drilling. SPE European Formation Damage Conference, Scheveningen, The Netherlands. Society of Petroleum Engineers. doi:10.2118/94763-MS.

Evje, S. and Wen, H. (2013, April). Weak solutions of a gas-liquid drift-flux model with general slip law for wellbore operations. Discrete Continuous Dynamic Systems, vol. 33, no. 10, pp. 4497–4530.

Gavrilyuk, S.L., and Fabre J. (1996, June). Lagrangian coordinates for a drift-flux model of a gas-liquid mixture. International Journal of Multiphase Flow, Volume 22, Issue 3, June 1996, Pages 453-460, ISSN 0301-9322.

Godhavn, J.-M. (2010, September 1). Control Requirements for Automatic Managed Pressure Drilling System. SPE Drilling and Completion. Society of Petroleum Engineers. doi:10.2118/119442-PA.

Guo, B. and Liu, G. (2011). Applied Drilling Circulation Systems: Hydraulics, Calculations and Models. Gulf Professional Publishing.

Gravdal, J. E., Nikolaou, M., Breyholtz, Ø., & Carlsen, L. A. (2010, December 1). Improved Kick Management During MPD by Real-Time Pore-Pressure Estimation. SPE Drilling and Completion. Society of Petroleum Engineers. doi:10.2118/124054-PA.

Hauge, E., Aamo, O. M., and Godhavn, J.-M. (2012, June). Model-based Estimation and Control of In/Out-flux During Drilling. Proceedings of American Control Conference, pp. 4909-4914.

Hauge, E., Aamo, O. M., and Godhavn, J.-M. (2013). Application of an Infinite-Dimensional Observer for Drilling System Incorporating Kick and Loss Detection. Proceedings of European Control Conference, pp. 1065-1070.

Kaasa, G.-O., Stamnes, Ø. N., Aamo, O. M., & Imsland, L. S. (2012, March 1). Simplified Hydraulics Model Used for Intelligent Estimation of Downhole Pressure for a Managed-Pressure-Drilling Control System. SPE Drilling and Completion. Society of Petroleum Engineers. doi:10.2118/143097-PA.

Karimi Vajargah, A. (2013, December). Pressure Signature of Gas Influx. PhD thesis. University of Tulsa.

Karimi Vajargah, A., Hoxha, B. B., and van Oort, E. (2014, September 10). Automated Well Control Decision-Making during Managed Pressure Drilling Operations. SPE Deepwater Drilling and Completions Conference, Galveston, Texas. Society of Petroleum Engineers doi:10.2118/170324-MS.

Kinik, K., Gumus, F., and Osayande, N. (2015, April 1). Automated Dynamic Well Control With Managed-Pressure Drilling: A Case Study and Simulation Analysis. SPE Drilling and Completion. Society of Petroleum Engineers. doi:10.2118/168948-PA.

Ljung, L. (1999) System identification: theory for the user, 2nd Edition. Upper Saddle River, Prentice-Hall.

Masella, J., Tran, Q., Ferre, D, and Pauchon, C. (1998, August). Transient simulation of two-phase flows in pipes. In: International. Journal of Multiphase Flow. 24. 5 pp. 739–755.

Nickens, H.V. (1987, June). A Dynamic Computer Model of a Kicking Well. SPE Drilling Engineering, pp. 158–173.

Petersen, J., Rommetveit, R., Bjorkevoll, K. S., & Froyen, J. (2008, August 25-27). A General Dynamic Model for Single and Multi-phase Flow Operations during Drilling, Completion, Well Control and Intervention. IADC/SPE Asia Pacific Drilling Technology Conference and Exhibition, Jakarta, Indonesia. Society of Petroleum Engineers. doi:10.2118/114688-MS.

Podio, A. L., and Yang, A. P. (1986, February 10-12). Well Control Simulator for IBM Personal Computer. Paper IADC/SPE 14737, presented at the IADC/SPE Drilling Conference held in Dallas, Texas.

Pournazari, P., Ashok, P., van Oort, E., Unrau, S., & Lai, S. (2015, September 15). Enhanced Kick Detection with Low-Cost Rig Sensors Through Automated Pattern Recognition and Real-Time Sensor Calibration. SPE Middle East Intelligent Oil and Gas Conference and Exhibition, Abu Dhabi, UAE. Society of Petroleum Engineers. doi:10.2118/176790-MS.

Reitsma, D., and Couturier, Y. (2012). New Choke Controller for Managed Pressure Drilling. 2012 IFAC Workshop on Automatic Control in Offshore Oil and Gas Production. Volume 1, Part 1, pp. 223-230. doi: 10.3182/20120531-2-NO-4020.00049.

Rommetveit, R. and Vefring, E. H. (1991, October 6-9). Comparison of Results from an Advanced Gas Kick Simulator with Surface and Downhole Data from Full Scale Gas Kick Experiments in an Inclined Well. Paper SPE 22558 presented at the 66th Annual Technical Conference and Exhibition of the Society of Petroleum Engineers, Dallas, Texas.

Santos, H., Leuchtenberg, C., & Shayegi, S. (2003, April 27-30). Micro-Flux Control: The Next Generation in Drilling Process. SPE Latin American and Caribbean Petroleum Engineering Conference, Port-of-Spain, Trinidad and Tobago. Society of Petroleum Engineers. doi:10.2118/81183-MS.

Shayegi, S., Kabir, C. S., If, F., Christensen, S., Ken, K., Casasus-Bribian, J., Moos, D. (2012, March 1). Reservoir Characterization Begins at First Contact With the Drill Bit. SPE Drilling and Completion. Society of Petroleum Engineers. doi:10.2118/159247-PA.

Shi, H., Holmes, J. A., Durlofsky, L. J., Aziz, K., Diaz, L., Alkaya, B., and Oddie, G. (2005, March 1). Drift-Flux Modeling of Two-Phase Flow in Wellbores. SPE Journal. Society of Petroleum Engineers. doi:10.2118/84228-PA.

Suryanarayana, P. V., Kennedy, Vaidya, R. N., & Wind, J. (2007, March 31). Use of a New Rate-Integral Productivity Index in Interpretation of Underbalanced Drilling Data for Reservoir Characterization. 2007 Production Operations Symposium, Oklahoma City, Oklahoma. Society of Petroleum Engineers. doi:10.2118/106756-MS.

Taitel, Y., Shoham, O., and Brill, J. (1989). Simplified transient solution and simulation of two-phase flow in pipelines. Chemical Engineering Science, vol. 24, no. 6, pp. 1353-1359.

Vefring, E. H., Nygaard, G., Lorentzen, R. J., Nævdal, G., & Fjelde, K. K. (2003, March 25-26). Reservoir Characterization during UBD: Methodology and Active Tests. IADC/SPE Underbalanced Technology Conference and Exhibition. Houston, Texas. Society of Petroleum Engineers. doi:10.2118/81634-MS.

Wiggins, M. L., Russell, J. E., and Jennings, J. W. (1996, December 1). Analytical Development Of Vogel-Type Inflow Performance Relationships. SPE Journal. Society of Petroleum Engineers. doi:10.2118/23580-PA.

Zhou, J., Stamnes, Ø.N., Aamo, O.M., and Kaasa, G.-O. (2011, March), Switched Control for Pressure Regulation and Kick Attenuation in a Managed Pressure Drilling System. IEEE Transactions on Control Systems Technology, vol.19, no.2, pp.337-350, doi: 10.1109/TCST.2010.2046517.

Appendix A. Derivation of the Reduced Drift-Flux Model

The derivation starts from the classical two-phase Drift-Flux formulation (Gavrilyuk and Fabre, 1996):

$$\frac{\partial(\alpha_L\rho_L)}{\partial t}+\frac{\partial(\alpha_L\rho_L v_L)}{\partial x}=\Gamma_L, \tag{A1}$$

$$\frac{\partial(\alpha_G\rho_G)}{\partial t}+\frac{\partial(\alpha_G\rho_G v_G)}{\partial x}=\Gamma_G, \tag{A2}$$

$$\frac{\partial(\alpha_L\rho_L v_L+\alpha_G\rho_G v_G)}{\partial t}+\frac{\partial(P+\alpha_L\rho_L v_L^2+\alpha_G\rho_G v_G^2)}{\partial x}=S, \tag{A3}$$

where $\alpha_i, v_i, \rho_i, \Gamma_i$ are volume fraction, velocity, density and mass source terms, for the gas and liquid phases (denoted by subscripts G and L, respectively), and S is the momentum source term, defined as:

$$S=\ -\rho_m g cos\theta-\frac{2f\rho_m v_m|v_m|}{D}, \tag{A4}$$

where $\rho_m,\ v_m$ can be found from the mixture relations:

$$\rho_m=\alpha_G\rho_G+\alpha_L\rho_L;\ v_m=\alpha_G v_G+\alpha_L v_L \tag{A5}$$

In the above, Eqs. A1-A2 represent the gas and liquid mass balances, respectively, and Eq. A3 is the momentum balance. The gas and liquid velocities are related through the slip law:

$$v_G=C_0 v_m+v_\infty=\frac{\alpha_G v_G+\alpha_L v_L}{1-\alpha_L^*}+v_\infty, \tag{A6}$$

where we define the profile parameter $\alpha_L^*\equiv\ (C_0-1)/C_0$, and the slip velocity v_∞. Several correlations exist for computing $C_0$and v_∞ (see e.g. Choi et al., (2012), Bhagwat and Ghajar (2014)), in our case we are assuming that C_0 is constant and v_∞ is obtained using the Shi et al. (2005) model, detailed in Appendix B. We also note the closure relations:

$$\alpha_G+\alpha_L=1 \tag{A7}$$

and

$$P=Z_G\rho_G R_G T. \tag{A8}$$

Eq. A8 is the gas equation of state, where the compressibility factor, Z_G, can be computed as a function of the pressure and temperature profile in the well (for instance, the Hall-Yarborough correlation (Ahmed, 2006) may be used).

The following assumptions and simplifications are made for the reduced DFM derivation:

1. The liquid phase density is constant. In practice, this will not be the case, as density varies with pressure and temperature, but an average value could be taken over the length of the well.
2. Distributed pressure transients are neglected. This assumption is justified by the fact that void wave propagation is typically several orders of magnitude slower than pressure wave propagation in drilling fluids (Masella et al., 1998).
3. When computing the frictional pressure drop, a uniform mixture velocity is used.
4. When computing the gas velocity profile, pressure transients are neglected.

The derivation starts with the following relation, found by rewriting the slip law (Eq. A6):

$$\alpha_L v_L = (\alpha_L - \alpha_L^*) v_G - (1 - \alpha_L^*) v_\infty. \tag{A9}$$

Substituting Eq.A9 into Eq. A1, with the assumption of constant ρ_L and $\frac{\partial[(1-\alpha_L^*)v_\infty]}{\partial x} \cong 0$, we get:

$$\frac{\partial \alpha_L}{\partial t} + \frac{\partial[(\alpha_L - \alpha_L^*) v_G]}{\partial x} = \frac{\Gamma_L}{\rho_L}, \tag{A10}$$

which, after applying the product rule for derivatives, combined with Eq. A7, yields:

$$\frac{\partial \alpha_G}{\partial t} + v_G \frac{\partial \alpha_G}{\partial x} = (\alpha_L - \alpha_L^*) \frac{\partial v_G}{\partial x} - \frac{\Gamma_L}{\rho_L}. \tag{A11}$$

From Eq. A2, we can apply the product rule to obtain the following relationship:

$$\frac{\partial v_G}{\partial x} = \frac{\Gamma_G}{\alpha_G \rho_G} - \frac{1}{\rho_G}\left(\frac{\partial \rho_G}{\partial t} + v_G \frac{\partial \rho_G}{\partial x}\right) - \frac{1}{\alpha_G}\left(\frac{\partial \alpha_G}{\partial t} + v_G \frac{\partial \alpha_G}{\partial x}\right). \tag{A12}$$

Inserting Eq. A12 into the right-hand side of Eq. A11 results, after algebraic manipulation, in:

$$\frac{\partial \alpha_G}{\partial t} + v_G \frac{\partial \alpha_G}{\partial x} = E_G + \Gamma_G^* - \Gamma_L^*, \tag{1}$$

where we define the following variables:

$$E_G \equiv -\frac{\alpha_G(\alpha_L - \alpha_L^*)}{(1 - \alpha_L^*)\rho_G}\left(\frac{\partial \rho_G}{\partial t} + v_G \frac{\partial \rho_G}{\partial x}\right); \Gamma_G^* \equiv \frac{\alpha_L - \alpha_L^*}{1 - \alpha_L^*} \frac{\Gamma_G}{\rho_G} \; ; \; \Gamma_L^* \equiv \frac{\alpha_G}{1 - \alpha_L^*} \frac{\Gamma_L}{\rho_L}. \tag{A13}$$

where E_G can be interpreted as the local gas expansion rate inside a grid cell, while Γ_G^* and Γ_L^* are contributions of the mass source terms to the overall gas dynamics.
Using the variables defined in Eq. A13, we can simplify Eq. A12 as:

$$\frac{\partial v_G}{\partial x} = \frac{E_G + \Gamma_G^*}{\alpha_L - \alpha_L^*} + \frac{1}{1-\alpha_L^*}\frac{\Gamma_L}{\rho_L}. \tag{A14}$$

The boundary condition for Eq. 1, defined at the bottom of the well (*x=0*), is:

$$\alpha_G(0,t) = \frac{q_G}{A v_{G0}}, \tag{12}$$

where

$$v_{G0} \equiv v_G(0,t) = C_0 \frac{q_G + q_L}{A} + v_\infty, \tag{7}$$

with q_G, q_L gas and liquid injection rates, respectively. The result in Eq. 7 was derived from the slip law (Eq. A6) by setting $v_m = \frac{q_G+q_L}{A}$.

Next, we derive a relationship between gas phase density and pressure, in the form of:

$$\frac{d\rho_G}{\rho_G} = \frac{dP}{\gamma P}, \tag{A15}$$

where $\gamma = 1$ for the isothermal case, and γ is equal to the adiabatic gas constant for an isentropic process. $\gamma = 1.3$ is used in the simulations (assuming methane at standard temperature conditions). The relation in Eq. A15 allows us to write the gas expansion rate in terms of pressure and its time and space derivatives:

$$E_G \equiv -\frac{\alpha_G(\alpha_L - \alpha_L^*)}{(1-\alpha_L^*)\gamma P}\left(\frac{\partial P}{\partial t} + v_G \frac{\partial P}{\partial x}\right) = -\frac{\alpha_G(1 - C_0\alpha_G)}{\gamma P}\left(\frac{\partial P}{\partial t} + v_G \frac{\partial P}{\partial x}\right). \tag{A16}$$

We can also write the mass source term Γ_G^* as a function of pressure, using the relationship $c_G^2 = \frac{\gamma P}{\rho_G}$

$$\Gamma_G^* = \frac{\alpha_L - \alpha_L^*}{1-\alpha_L^*}\frac{c_G^2 \Gamma_G}{\gamma P}. \tag{A17}$$

The pressure gradient, $\frac{\partial P}{\partial x}$, can be calculated by imposing a static momentum balance in place of Eq. A3:.

$$\frac{\partial P}{\partial x} = \bar{S}(x) = -(\rho_L a_L + \bar{\rho}_G \alpha_G)\left[g\cos\theta + \frac{2f(q_G+q_L)|q_G+q_L|}{A^2 D}\right], \tag{9}$$

where a mean or approximated gas density $\bar{\rho}_G$ needs to be used since pressure is implicitly dependent on gas density (from Eq. A8). For instance, $\bar{\rho}_G$ may be computed from Eq. A8 assuming a linear temperature

profile, and the pressure profile at the previous time instant. Integrating Eq. 9 from wellbore depth, *x*, to the top side (*x=L)* gives

$$P(x) = P_c + \int_L^x \bar{S}(\xi)d\xi, \tag{8}$$

where $P(x = L) = P_c$. The friction factor, *f*, in Eq. 9 is calculated from yield-power law fluid correlations for the annulus (Ahmed and Miska, 2009).

Having obtained an expression for $\partial P/\partial x$, we can further simplify the gas velocity expression (Eq. A14). Using Eq. A16-A17 together with Eq. 9, and the fact that $C_0 = \frac{1}{1-\alpha_L^*}$, yields:

$$\frac{\partial v_G}{\partial x} = C_0\left(-\frac{\alpha_G v_G}{\gamma P}\bar{S} - \frac{\alpha_G}{\gamma P}\frac{\partial P}{\partial t} + \frac{c_G^2}{\gamma P}\Gamma_G + \frac{\Gamma_L}{\rho_L}\right). \tag{A19}$$

If we further neglect $\partial P/\partial t$ when computing the velocity gradient, we have the approximation

$$\frac{\partial v_G}{\partial x} \approx C_0\left(-\frac{\alpha_G v_G}{\gamma P}\bar{S} + \frac{c_G^2}{\gamma P}\Gamma_G + \frac{\Gamma_L}{\rho_L}\right). \tag{A20}$$

Integrating Eq. A20 over the length of the well, we get:

$$v_G(x) = e^{-I_v(x)}\left(v_{G0} + C_0\int_0^x \left[\frac{c_G^2(\zeta)}{\gamma P(\zeta)}\Gamma_G(\zeta) + \frac{\Gamma_L(\zeta)}{\rho_L}\right] e^{I_v(\zeta)}d\zeta\right), \tag{10}$$

where

$$I_v(x) = \int_0^x \frac{C_0\alpha_G(\xi)}{\gamma P(\xi)}\bar{S}(\xi)d\xi. \tag{11}$$

Furthermore, by neglecting the distributed pressure transients, we can assume that $\partial P/\partial t \approx dP_c/dt$. The pressure dynamics at the wellhead are formulated using a lumped expression, similar to the one used by Zhou et al. (2011)

$$\frac{dP_c}{dt} = \frac{\beta_L}{V}(q_L + q_G + T_{E_G} - q_c), \tag{A21}$$

where the T_{E_G} term accounts for the gas expansion in the well, which can be obtained by integrating the gas velocity gradient (Eq. A19) times the cross-sectional area over the length of the well (note that here we include the term $\partial P/\partial t \approx dP_c/dt$):

$$T_{E_G} = \int_0^L AC_0\left(-\frac{\alpha_G v_G}{\gamma P}\bar{S} + \frac{c_G^2}{\gamma P}\Gamma_G + \frac{\Gamma_L}{\rho_L}\right)dx - \frac{dP_c}{dt}\int_0^L A\frac{C_0\alpha_G}{\gamma P}dx. \tag{A22}$$

If we define

$$T_{XE} \equiv \int_0^L AC_0 \left(-\frac{\alpha_G v_G}{\gamma P} \bar{S} + \frac{c_G^2}{\gamma P} \Gamma_G + \frac{\Gamma_L}{\rho_L} \right) dx = A(v_G(L) - v_{G0}), \tag{6}$$

and substitute Eq. A22 into Eq. A21, then bring the $\frac{dP_c}{dt}$ term to the left hand side of Eq. A21, we have:

$$\frac{dP_c}{dt} \left(1 + \frac{\beta_L}{V} \int_0^L \frac{C_0 \alpha_G}{\gamma P} A dx \right) = \frac{\beta_L}{V} (q_L + q_G - q_c + T_{XE}). \tag{A23}$$

Finally, if we define the effective bulk modulus

$$\bar{\beta} \equiv \frac{\beta_L}{1 + \frac{\beta_L}{V} \int_0^L \frac{C_0 \alpha_G}{\gamma P} A dx}, \tag{5}$$

we obtain the final equation:

$$\frac{dP_c}{dt} = \frac{\bar{\beta}}{V} (q_L + q_G - q_c + T_{XE}). \tag{2}$$

Appendix B. Slip Model

From Shi et al. (2005), we can calculate the slip velocity between the gas and liquid phases, according to:

$$v_\infty = \frac{(1 - \alpha_G C_0) C_0 K(\alpha_G) v_{cr}}{\alpha_G C_0 \sqrt{\frac{\rho_G}{\rho_L}} + 1 - \alpha_G C_0}, \tag{B1}$$

where

$$v_{cr} = \left[\frac{\sigma g (\rho_L - \rho_G)}{\rho_L^2} \right]^{\frac{1}{4}}, \tag{B2}$$

$$K(\alpha_G) = \begin{cases} \dfrac{1.53}{C_0}, & \alpha_G \le 0.2 \\ 3.182 \left(1 - e^{-\frac{D'}{9.3833}} \right), & \alpha_G > 0.4 \end{cases}, \tag{B3}$$

with

$$D' = \sqrt{\frac{g(\rho_L - \rho_G)}{\sigma}} D \tag{B4}$$

and C_0 the slip law profile parameter. For $0.2 \leq \alpha_G < 0.4$, the $K(\alpha_G)$ value can be obtained by linear interpolation between the two expressions in Eq. B3.

Appendix C. Recursive Least Squares Algorithm

We start from the linear model

$$y = \phi^T X, \tag{C1}$$

where y and ϕ represent measured parameters (y is a scalar, while ϕ is a vector) and X is the vector of unknown parameters. If we denote $\hat{X}(t)$ as the time-varying estimate of X, $\boldsymbol{P}(t)$ the covariance matrix and $0 < \lambda \leq 1$ the forgetting factor, we have the RLS scheme (Ljung, 1999):

$$\boldsymbol{P}(t) = \frac{1}{\lambda}[\boldsymbol{P}(t-1) - \epsilon(t)\phi^T(t)\boldsymbol{P}(t-1)], \tag{C2}$$

$$\hat{X}(t) = \hat{X}(t-1) + \epsilon(t)\big[y(t) - \phi^T(t)\hat{X}(t-1)\big], \tag{C3}$$

with:

$$\epsilon(t) = \boldsymbol{P}(t-1)\phi(t)[\lambda + \phi^T(t)\boldsymbol{P}(t-1)\phi(t)]^{-1}. \tag{C4}$$

Appendix D. Numerical Scheme

The reduced DFM equations are discretized using an explicit algorithm consisting of a first-order upwind scheme in space and the forward Euler method in time. In discretized form, Eq. 1 becomes, using the notation $\alpha_G(i,n) = \alpha_G(i\Delta x, n\Delta t)$, with the cell index $i = 1,2,..,N$, and the time index $n = 1,2,$ ...:

$$\frac{\alpha_G(i,n+1) - \alpha_G(i,n)}{\Delta t} + \max(v_G(i,n),0)\left[\frac{\alpha_G(i,n) - \alpha_G(i-1,n)}{\Delta x}\right] + \min(v_G(i,n),0)\left[\frac{\alpha_G(i+1,n) - \alpha_G(i,n)}{\Delta x}\right] = E_G(i.n) + \Gamma_G^*(i,n) - \Gamma_L^*(i,n), \tag{D1}$$

where

$$E_G(i.n) = -\frac{\alpha_G(i,n)(1 - C_0\alpha_G(i.n))}{\gamma P(i,n)}\left(\frac{\bar{\beta}(n)}{V}[q_L(n) + q_G(n) - q_c(n) + T_{XE}(n)] + v_G(i,n)\bar{S}(i,n)\right), \tag{D2}$$

$$\Gamma_G^* \equiv \frac{(1 - C_0\alpha_G)c_G^2(i)\Gamma_G(i,n)}{\gamma P(i.n)}; \quad \Gamma_L^* \equiv \frac{\mathrm{C_0\alpha_G}(i,n)\Gamma_L(i,n)}{\rho_L}, \tag{D3}$$

$$P(i,n) = P_c(n) - \sum_{\xi=i}^{N} \bar{S}(\xi,n)\,\Delta x, \tag{D4}$$

$$\bar{S}(i,n) = -(\rho_L a_L(i.n) + \bar{\rho}_G(i,n)\alpha_G(i.n))\left[gcos(\theta(i)) + \frac{2f\left(q_G(n) + q_L(n)\right)^2}{A^2 D}\right], \tag{D5}$$

$$\bar{\rho}_G(i,n) = \frac{P(i,n-1)}{Z_G(i,n-1)R_G T(i)}, \tag{D6}$$

$$v_G(i,n) = e^{-I_v(i.n)}\left(v_G(1,n) + C_0\sum_{\zeta=1}^{i}\left[\frac{c_G^2(i)}{\gamma P(\zeta,n)}\Gamma_G(\zeta,n) + \frac{\Gamma_L(\zeta,n)}{\rho_L}\right] e^{I_v(\zeta,n)}\,\Delta x\right), \tag{D7}$$

$$I_v(i,n) = \sum_{\xi=1}^{i}\left[\frac{C_0\alpha_G(\xi,n)}{\gamma P(\xi,n)}\bar{S}(\xi,n)\right]\Delta x, \tag{D8}$$

$$v_G(1,n) = \frac{C_0}{A}[q_G(n) + q_L(n)] + v_\infty, \tag{D9}$$

with the boundary condition

$$\alpha_G(1,n) = \frac{q_G(n)}{A v_G(1,n)}, \tag{D10}$$

Finally, Eq. 2 is discretized, with $P_c(n) = P_c(n\Delta t)$, using the explicit Euler method:

$$\frac{P_c(n+1) - P_c(n)}{\Delta t} = \frac{\bar{\beta}(n)}{V}[q_L(n) + q_G(n) - q_c(n) + T_{XE}(n)], \tag{D11}$$

where

$$\bar{\beta}(n) = \frac{\beta_L}{1 + \frac{\beta_L}{V}\sum_{\xi=1}^{N}\left[\frac{C_0 \alpha_G(\xi.n)}{\gamma P(\xi.n)} A\right] \Delta x}, \tag{D12}$$

$$T_{XE} = A(v_G(N,n) - v_G(1,n)). \tag{D13}$$